New insights into the mechanism of phosphate release during particulate organic matter photodegradation based on optical and molecular signatures

Minli Guo, Xiaolu Li, Yi Wang, Yunlin Zhang, Qinglong Fu, Arnaud Huguet, Guanglong Liu

Graphical abstract

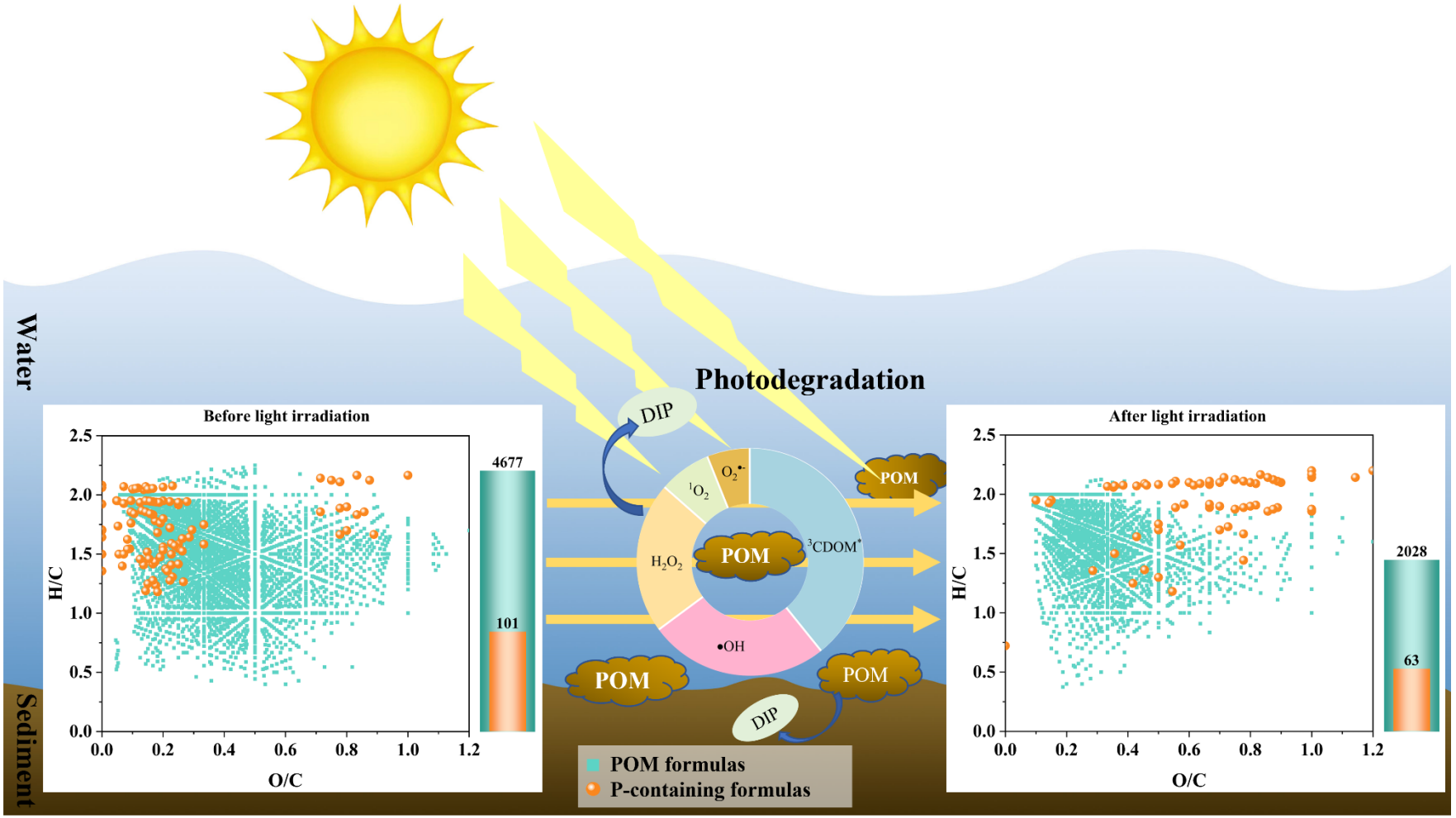

Highlights:

• Phosphate release during POM photodegradation was characterized by FT-ICR MS.

• Organic phosphorus in POM participated in the photochemical reactions.

• Unsaturated P-containing formulas in POM were preferentially photodegraded.

• ^{3}CDOM* was mainly responsible for POM photodegradation in aquatic environment.

New insights into the mechanism of phosphate release during particulate organic matter photodegradation based on optical and molecular signatures

Minli Guo[a], Xiaolu Li[a], Yi Wang[a], Yunlin Zhang[b], Qinglong Fu[c], Arnaud Huguet[d], Guanglong Liu[a*]

Affiliations

[a]Key Laboratory of Arable Land Conservation (Middle and Lower Reaches of Yangtze River), Ministry of Agriculture and Rural Affairs, College of Resources and Environment, Huazhong Agricultural University, Wuhan 430070, China

[b]State Key Laboratory of Lake Science and Environment, Nanjing Institute of Geography and Limnology, Chinese Academy of Sciences, Nanjing 210008, China

[c]School of Environmental Studies, China University of Geosciences, Wuhan 430074, China

[d]Sorbonne Université, CNRS, EPHE, PSL, UMR METIS, F-75005 Paris, France

*Corresponding author.

E-mail address: liugl@mail.hzau.edu.cn (Guanglong Liu)

Abstract

Phosphate release from particulate organic matter (POM) dominates phosphorus (P) cycling in aquatic ecosystems. However, the mechanisms underlying P release from POM remain poorly understood because of complex fractionation and analytical challenges. In this study, the release of dissolved inorganic phosphate (DIP) during POM photodegradation was assessed using excitation–emission matrix (EEM) fluorescence spectroscopy and Fourier transform ion cyclotron resonance mass spectrometry (FT-ICR MS). POM in suspension was significantly photodegraded under light irradiation, concomitantly with the production and release of DIP in the aqueous solution. Chemical sequential extraction revealed that organic phosphorus (OP) in POM participated in photochemical reactions. Moreover, FT-ICR MS analysis revealed that the average molecular weight of P-containing formulas decreased from 374.2 to 340.1 Da. Formulas containing P with a lower oxidation degree and unsaturation were preferentially photodegraded, generating oxygen-enriched and saturated formula compounds, such as protein- and carbohydrate-like P-containing formulas, benefiting further utilization of P by organisms. Reactive oxygen species played an important role in the photodegradation of POM, and excited triplet state chromophoric dissolved organic matter ($^{3}CDOM^{*}$) was mainly responsible for POM photodegradation. These results provide new insights into the P biogeochemical cycle and POM photodegradation in aquatic ecosystems.

Keywords: Particulate organic matter; Photodegradation; Phosphate; FT-ICR MS; Reactive oxygen species

Abbreviations

POM, particulate organic matter; DIP, dissolved inorganic phosphate; EEM, excitation–emission matrix; FT-ICR MS, Fourier transform ion cyclotron resonance mass spectrometry; OP, organic phosphorus; $^{3}CDOM^{*}$, excited triplet state chromophoric dissolved organic matter; ROS, reactive oxygen species; OM, organic matter; DOP, dissolved organic phosphorus; SPE, solid phase extraction; TOC, total organic carbon; TMP, 2,4,6-trimethyphenol; FFA, furfuryl alcohol; •OH, hydroxyl radical; $O_2^{\bullet-}$ superoxide anion; $^{1}O_2$, singlet oxygen; KMD, Kendrick mass defect; DBE, double bond equivalent; CNs, carbon numbers; DOM, dissolved organic matter

1. Introduction

Frequent water blooms caused by eutrophication pose a major threat to ecological health and drinking water safety (Hou et al., 2022; Zhang et al., 2022b). Phosphorus (P) is the key element involved in eutrophication and algal blooms (Conley et al., 2009; Schindler et al., 2016). After the efficient control of exogenous P input, the rapid transformation of endogenous P has become an important source of P compensation (Xu et al., 2018). The transport and transformation of particulate organic matter (POM), a carrier of endogenous P, can greatly impact the amount of bioavailable P in water (Joshi et al., 2015; Li et al., 2017a). Accelerated eutrophication of water bodies accumulates a large amount of POM, and the decomposition of POM through mineralization or abiotic processes can release a large amount of dissolved nutrients, compensating for the P demand during phytoplankton growth.

Traditionally, research has been focused on the biomineralization process of POM, in which microorganisms play an important role (Zhang et al., 2022a). Recent studies have revealed that photochemical transformation is also important for the fate of POM (Harfmann et al., 2021; Helms et al., 2014; Lee et al., 2021; Liu and Shank, 2015). The photochemical transformation of POM caused by solar radiation can change its chemical composition and molecular size and ultimately affect the biogeochemical processes of carbon (C), nitrogen (N), and P (Hu et al., 2022; Lee et al., 2023; Mayer et al., 2006). Previous studies have also confirmed that POM can be photodegraded and release dissolved nutrients and that this process can be affected by irradiation conditions, POM properties, reactive oxygen species (ROS), and other factors (Hu et al., 2021;

74 Shank, 2011). Our previous research revealed that suspended particles in shallow lakes
75 can release dissolved inorganic phosphate (DIP) under sunlight exposure (Guo et al.,
76 2020; Li et al., 2019). Its release mechanism involves photolysis, enzymatic hydrolysis
77 of organic phosphorus (OP), and catalytic hydrolysis by minerals (Baldwin et al., 1995;
78 Klein et al., 2019; Wan et al., 2019). However, the extractants used in chemical
79 sequential extraction lack specificity (Zhu et al., 2013). Moreover, the peak spectrum
80 in ^{31}P-nuclear magnetic resonance (^{31}P-NMR) is easy to overlap (Worsfold et al., 2008),
81 resulting in insufficient understanding of the mechanism of DIP release during POM
82 photodegradation.

83 Fourier transform ion cyclotron resonance mass spectrometry (FT-ICR MS) is a
84 robust tool for analyzing complex organic matter (OM) at the molecular level, despite
85 its complexity and heterogeneity. This ultra-high-resolution technique is powerful to
86 determine the molecular composition of complex environmental samples (Bahureksa
87 et al., 2021) and has been widely used for the molecular characterization of OM in
88 various types of environmental samples (Kellerman et al., 2015; McDonough et al.,
89 2022; Singer et al., 2012; Wagner et al., 2015). Because OP molecules in the
90 environment are composed of ester (C-O-P) and carbon phosphorus (C-P) (Ni et al.,
91 2022), a few scholars have successfully used FT-ICR MS to analyze the source,
92 composition, and transformation of OP in the environment (Brooker et al., 2018; Gao
93 et al., 2021; Ni et al., 2021). The use of this technology greatly helps understand the P
94 biogeochemical cycle at the molecular level.

95 This study aimed to investigate DIP release resulting from POM photodegradation

in water, focusing on molecular changes occurring during this process. POM photodegradation and DIP release were assessed through a simulated light experiment. The molecular weight distribution, species, and structure of P-containing formulas in POM during photodegradation were analyzed using FT-ICR MS. In addition, ROS involved in POM photodegradation were investigated using a reactive oxygen molecular probe to obtain key results on the molecular mechanisms underlying DIP release during the photochemical transformation of POM.

2. Materials and Methods

2.1. Photodegradation experiments

A suspension of lake water and sediments was used to simulate the photodegradation of POM in shallow lakes. Lake water and sediment samples were collected from Lake Nanhu (Wuhan, China) on March 17, 2019. Basic information on Lake Nanhu is provided in the Supporting Information. The weather was bright, and the wind speed was 3.4–5.6 m/s in the week before sampling. The water sample was obtained from the overlying 10 cm surface of the lake. The top 10 cm sediment was collected using a Peterson grab collector. All water and sediment samples were screened for impurities and were mixed, covered with ice packs, and stored at 4 °C and −20 °C, respectively. The overlying water samples collected from each sampling site were filtered using 0.45 μm filters (Jinteng Experimental Equipment Co., Ltd, Tianjin, China) and stored at 4 °C. The basic physical and chemical parameters of the lake water and sediment samples are summarized in Table S1.

Wet sediment (4 g, moisture content: 34.63% ± 0.05%) was added to filtered lake

water (1 L) in a beaker and completely resuspended by stirring at 350 rpm for 16 h. The suspension (approximately 500 mg/L suspended particles) was then allowed to settle for 20 min, and the top 20 cm was collected for conducting photodegradation experiments in a rotating photoreactor (Phchem III, Newport Corporation, Beijing, China). A schematic of the experimental setups has been provided in our previous study (Guo et al., 2020). A high-pressure mercury lamp (300 W) was used to provide light, and a UV light photometer (UV254, Newport Corporation, Beijing, China) was used to measure the irradiance on the surface of the quartz tubes. The irradiation intensity was measured to be approximately 3.5 mW/cm^2, which was close to that on the lake water surface on a midsummer day. The internal temperature of the reactor was maintained at 35 ± 2 °C by connecting it with a quartz cold trap and a ventilation device. Before light irradiation, the magnetic stirrer was turned on overnight to ensure that the particles in suspension in the photochemical reaction tubes were in a completely suspended state and weakly adsorbed P was completely released. Samples were collected at scheduled time intervals to analyze the concentration of DIP. Dark treatment was set as a control and performed under the same conditions but by wrapping in tinfoil. To clarify the contribution of POM photodegradation to DIP concentrations in water, filtered lake water samples under light and dark treatments were used as controls.

2.2. Determination of P content

The amount of DIP released from POM photodegradation was determined using the molybdenum blue colorimetric method (Murphy and Riley, 1962). The dissolved total phosphorus (DTP) content was measured after digestion with 5% potassium

persulfate. The dissolved organic phosphorus (DOP) content was calculated by subtracting DIP from DTP.

To assess the changes in P components during POM photodegradation, the P fractions before and after light irradiation were analyzed by chemical sequential extraction, as proposed by Rydin (2000). Details of the method can be found in Fig. S1. Using this method, P was separated into six groups: NH_4Cl-P (loosely adsorbed P), BD-P (P forms sensitive to low redox potential, adsorbed to iron and manganese), NaOH-rP (P exchangeable with OH^-, mainly aluminium oxide), NaOH-nrP (OP), HCl-P (P forms sensitive to low pH, such as apatite), and Res-P (refractory organic P and the inert inorganic P fraction).

2.3. Pretreatment of POM and excitation–emission matrix (EEM) analysis

To evaluate the photodegradation of POM in suspension under light irradiation, the fluorescence spectrum of POM was determined. POM was extracted as described previously (He et al., 2016). In brief, the suspended particles were collected using 0.45 μm filters (Jinteng Experimental Equipment Co., Ltd, Tianjin, China) before and after light irradiation for 58 h and then freeze dried before grinding. Next, 1.0 g of freeze-dried suspended particles were soaked in 0.1 mol/L of NaOH solution and shaken at 180 rpm at 25 °C for 24 h. The solutions were then centrifuged at 10,000 rpm for 20 min, and the supernatants were filtered through precombusted 0.22 μm glass fiber filters (Jinteng Experimental Equipment Co., Ltd, Tianjin, China). The filtrates were collected and stored at 4 °C for no more than 2 weeks until other analyses and solid phase extraction (SPE). The concentration of total organic carbon (TOC) was measured by a

TOC analyzer (Vario TOC Cube, Elementar, Germany).

The fluorescence spectroscopy of POM was obtained by scanning at an excitation wavelength of 220–450 nm (2 nm interval) and emission wavelength of 250–600 nm (1 nm interval) using the Shimadzu fluorescence spectrophotometer RF5301. Fluorescence regional integration (FRI) and parallel factor (PARAFAC) modeling analyses of the POM extract were performed on MATLAB R2018b. EEM fluorescence spectroscopy data were calibrated using an ultrapure water blank.

2.4. SPE and FT-ICR MS analysis

SPE was performed using a previously described method (Brooker et al., 2018). In brief, 500 mg Bond Elut PAX cartridges (Agilent Technologies, 12257506) were used to extract POM formulas and P-containing formulas from all samples. The cartridges were first washed with 20 mL LC–MS-grade methanol (Fisher, USA) and then washed with 20 mL of ultrapure water. While still wet, the filtrates, which were adjusted to pH ~10 using NH_4OH and HCOOH, were gravity filtered through conditioned PAX cartridges to collect and concentrate OM with molecular weight < 1000 Da. The cartridges were rinsed with 20 mL of 1% NH_4OH for the complete removal of Cl^- and other ions to minimize the interference of Cl on the formula assignment of P-containing formulas. Next, the cartridges were dried with ultrapure N_2 gas. The samples were eluted from the cartridges using 10 mL of LC–MS-grade methanol, followed by 10 mL of methanol with 5% formic acid. The elutes were combined into amber glassware and dried with N_2 gas. After redissolving the elutes using LC–MS-grade methanol, a 9.4 T Bruker Apex Ultra FT-ICR MS instrument

equipped with an Apollo II electrospray ion source was used for FT-ICR MS analysis in the negative-ion mode. Detailed information on the operating parameters and data processing is provided in the Supporting Information. In brief, a 1 mL aliquot of leachates was dried with N_2 gas and diluted using 50 mL of ultrapure water to measure the extraction efficiency of PAX cartridges.

Van Krevelen diagrams are typically used for FT-ICR MS data comparison. They can distinguish biomolecular chemical classes using O/C and H/C plots (Kim et al., 2003; Ohno et al., 2010). According to van Krevelen diagrams, compounds are generally classified into seven categories (Feng et al., 2016; Ni et al., 2021): (1) lipids ($1.5 \leq H/C \leq 2$, $0 \leq O/C \leq 0.3$), (2) proteins ($1.5 \leq H/C \leq 2.2$, $0.3 \leq O/C \leq 0.67$), (3) carbohydrates ($1.5 \leq H/C \leq 2.4$, $0.67 \leq O/C \leq 1.2$), (4) unsaturated hydrocarbons ($0.7 \leq H/C \leq 1.5$, $0 \leq O/C \leq 0.1$), (5) lignins ($0.7 \leq H/C \leq 1.5$, $0.1 \leq O/C \leq 0.67$), (6) tannins ($0.5 \leq H/C \leq 1.5$, $0.67 \leq O/C \leq 1.2$), and (7) condensed aromatic structures ($0.2 \leq H/C \leq 0.7$, $0 \leq O/C \leq 0.67$).

2.5. Capture and detection of ROS

To determine the contribution of different ROS types on POM photodegradation, a series of sacrificial experiments were performed. Isopropanol (IPA, 0.2%), superoxide dismutase (SOD, 1200 U/L), catalase (CAT, 20 U/L), 2,4,6-trimethyphenol (TMP, 10 mM), and furfuryl alcohol (FFA, 5 mM) were added to quench any hydroxyl radical (•OH), superoxide anion ($O_2^{\bullet-}$), H_2O_2, excited triplet state chromophoric dissolved organic matter ($^3CDOM^*$), and singlet oxygen ($^1O_2$) (Zeng et al., 2022; Zhang et al., 2019; Zheng et al., 2022), respectively. $O_2^{\bullet-}$ was qualitatively analyzed by determining

206 the content of diformazan (produced by $O_2^{\bullet-}$ and nitro blue tetrazolium chloride) at 530
207 nm using a UV spectrophotometer (Zong et al., 2020). The generated H_2O_2 was
208 quantified by the colorimetric method using cerous sulfate. The selective probe
209 compound FFA, at an initial concentration of 1 mM (Song and Jiang, 2020), was used
210 to capture $^1O_2$. The probe molecule for $^3CDOM^*$-TMP was added to the reaction
211 solution at an initial concentration of 1 mM (Song and Jiang, 2020). To measure the
212 •OH concentration, benzoic acid (BA) (1 g/L) was added to the system (Chen et al.,
213 2017). The concentrations of FFA, TMP, and *para*-hydroxybenzoic acid (PBA)
214 (generated by •OH and BA) were determined by high-performance liquid
215 chromatography (HPLC, Agilent 1260). The detailed parameters of HPLC analyses are
216 listed in the Supporting Information.

217 **3. Results and Discussion**

218 **3.1. Photodegradation of POM and variation in P content**

219 The fluorescence spectroscopy of POM under light irradiation and dark treatment
220 is shown in Fig. S2. The signal intensity and region volume sharply decreased after
221 light irradiation, while almost no change was noted after dark treatment (Fig. S2 and
222 Table S2), indicating that the fluorophoric POM components were degraded under light
223 irradiation. The concentration of TOC in the POM extract decreased from 198.78 mg/L
224 to 93.68 mg/L after light irradiation, and the degradation rate reached to 52.87%. In
225 addition, the PARAFAC model with two to seven components was assessed. Based on
226 the residual analysis and split-half analysis, three components, including the protein-
227 like component C1, microbial humic-like component C2, and terrestrial humic-like

component C3, were determined as the best fit (Fig. 1). The maximum fluorescence intensity (F_{max}) values of these three components significantly decreased after light irradiation. The microbial humic-like component C2 showed the highest decrease (55.3%), followed by the terrestrial humic-like component C3 (50.5%) and protein-like component C1 (42.6%), indicating the photodegradation property of POM. This property can affect the composition and fate of POM, thereby affecting the concentration of bioavailable nutrients in aquatic environments and the eutrophication process.

Fig. 2 shows the release of DIP during the photodegradation of POM in suspension. The concentration of DIP in the suspension increased under both light and dark treatments. In the dark treatment group, DIP increased by 0.06 mg/L, mainly because of the microbial mineralization of POM. In contrast, DIP increased by 0.35 mg/L in the light treatment group; this was approximately sixfold higher than that in the dark treatment group, indicating that more POM was degraded during light treatment. Considering the amount of DIP released in the filtered lake water after light treatment (only 0.03 mg/L) (Fig. 2a), it could be confirmed that POM was a significant potential source of P in water. Kinetic analysis revealed that DIP release during POM photodegradation fit the pseudo-second order reaction (Table S3 and Fig. S3), indicating that intermediates were produced. The analysis of DOP concentration during the reaction process also revealed that as the irradiation time increased, the DOP concentration initially increased and then gradually decreased (Fig. S4), indicating that DOP may play a more intermediate role during the photodegradation of POM. To

250 further clarify the effect of microorganisms on phosphate release during POM
251 degradation, flow cytometry was performed to determine the number of
252 microorganisms (living and dead bacteria) in the resuspended samples (Fig. S5 and
253 Table S4). The number of microorganisms during light treatment was lower than that
254 during dark treatment after 10 h, indicating that the increase in DIP concentration during
255 light treatment was due to the photochemical degradation of POM.

256 To determine the P components involved in the photodegradation of POM,
257 chemical sequential extraction was performed to analyze the P components in POM.
258 The contents of BD-P and NaOH-rP, important components of the P pool in POM, did
259 not change significantly before and after light irradiation, while that of NaOH-rP only
260 increased slightly (Fig. 2b). These findings suggest that BD-P and NaOH-rP are not the
261 sources of DIP release in solution. The NaOH-nrP component (organic bound P) of
262 POM significantly decreased after light irradiation (Fig. 2b), again indicating that OP
263 in POM degraded during light irradiation. Surprisingly, the Res-P content also
264 decreased significantly after light irradiation. Res-P consists of refractory OP and inert
265 inorganic P (Rydin, 2000). Although inert OP in Res-P is difficult to be biodegraded
266 (Benitez-Nelson, 2000), it can still undergo photochemical decomposition.

267 **3.2. Variations in molecular characteristics of OP**

268 The molecular weight distributions of POM and P-containing formulas in POM
269 before and after light irradiation are presented in Fig. 3. The median molecular mass of
270 POM and P-containing formulas decreased from 365, 381 Da to 339, 335 Da, indicating
271 that light irradiation resulted in the conversion of POM and P-containing formulas into

small molecules. The average molecular weight of P-containing formulas was 374.2 Da (Table S5), which is close to that reported by Ni et al. (2021). However, the number of P-containing formulas detected in our sample (101) was lower than that reported by Ni et al (75–670) (Ni et al., 2021). This may be related to the sample composition, pretreatment process, and data analysis.

The changes in P-containing formulas in POM before and after light irradiation are shown in Fig. 4. Before light irradiation, most P-containing formulas were lipid-, lignin-, and carbohydrate-like P-containing formula compounds, with a relative abundance (RA) of 46.5%, 18.8%, and 13.9%, respectively. This was followed by unsaturated hydrocarbon-like (5.0%) and protein-like (2.0%) P-containing formula compounds. No P-containing formulas were detected in the tannin- and condensed aromatic structure-like formula compounds. After light irradiation, lipid-, unsaturated hydrocarbon-, and lignin-like P-containing formula compounds were almost removed; their RA decreased by 94.6%, 94.4%, and 48.3%, respectively (Fig. S6). Some protein- and carbohydrate-like P-containing formula compounds with high O/C were newly generated (Fig. 4b). The H/C_{wa} of P-containing formulas increased from 1.78 to 2.01 and their O/C_{wa} increased from 0.20 to 0.75 after light irradiation (Table S5), indicating that P-containing formulas exhibited higher saturation and stronger oxidation after light irradiation. In summary, our results indicate that photochemical degradation tended to remove P-containing formula compounds in POM with a low oxygen content, such as lipid- and lignin-like P-containing formula compounds, and produce P-containing formula compounds with a high oxygen content, such as protein- and carbohydrate-like

P-containing formula compounds.

To illustrate the compositional changes occurring within each subcategory of molecules, photodegradable (peak lost), photogenerated (new peak), and photoresistant (peak retained) P-containing formulas after light irradiation are plotted in Fig. 5. Photodegradable P-containing formulas were mainly concentrated in the low O/C region (O/C < 0.3) and high H/C region (H/C > 1.0). In contrast, photogenerated P-containing formulas were mainly concentrated in the regions of O/C > 0.3 and H/C > 1.0. The quantitative distributions of photodegradable, photogenerated, and photoresistant P-containing formulas are presented in Fig. S7. These results suggest that (i) less oxidized (i.e., lower O/C) and more aliphatic (i.e., higher H/C) compounds were preferentially degraded to generate oxygen-rich molecules, explaining the significant increase in O/C values, and (ii) the degradation of different O/C and H/C fractions in P varied greatly. Therefore, the degradation potential of P-containing formula compounds can be predicted by determining the O/C and H/C ratios of different P sources.

The transformation of P molecules can be inferred from the two-dimensional display of Kendrick mass defect (KMD) versus nominal mass in FT-ICR MS (Hughey et al., 2001). Molecules with the same KMD value correspond to compounds belonging to the same class and type but with different numbers of functional groups (CH_2 groups in this study, alkyl chain length). The difference between compounds with the same KMD value but different mass values can be explained by the change in the number of CH_2, which represents the difference in the aliphatic properties of OM (Riedel et al., 2012). In other words, the longer the alkyl chain length (i.e., the more the number of

316 CH_2 groups), the stronger is the aliphatic property of OM. An increase or decrease in
317 the number of alkyl chain substituents of their homologous formula will
318 correspondingly increase or decrease the molecular weight.

319 Before light irradiation, P-containing formulas were evenly distributed in the
320 range of 250–480 Da (Fig. 6). After light irradiation, P-containing formulas with
321 different alkyl chain lengths were removed to varying degrees. In the homologous series,
322 P-containing formulas with higher mass values (greater than 400 Da) were
323 preferentially removed, which corresponded to the decrease in their molecular weights
324 (Table S5). When the KMD values were <0.25, P-containing formulas were almost
325 removed, indicating lower removal selectivity by light irradiation. This implies that P-
326 containing formulas with high molecular weights (stronger aliphatic property) and low
327 KMD values are preferentially removed by light irradiation. In addition, the intensity
328 of P-containing formulas decreased to varying degrees after light irradiation, also
329 indicating the photodegradation of P-containing formulas.

330 Double bond equivalent (DBE) is an important parameter to clarify the
331 unsaturation and aromaticity of organic compounds (Gao et al., 2021). The distribution
332 of DBE and carbon numbers (CNs) can be used to analyze and compare the
333 characteristics of oxygen-containing molecules in OM (Bae et al., 2011). The
334 relationship between the DBE and CNs of P-containing formulas is plotted in Fig. S8.
335 Before light irradiation, P-containing formulas had a wide DBE range of 0–9; this range
336 is lower than that of P-containing formula compounds (0–14) reported by Gao et al. in
337 various treatment units of a wastewater treatment plant (Gao et al., 2021). This indicates

that the P-containing formulas in our study had low unsaturation and low aromaticity, which also corresponded to the lower AI_{wa}. After light irradiation, formulas with DBE > 5 were largely removed and the DBE value sharply decreased, indicating an increase in double bonds (unsaturated hydrocarbons) or the opening of the benzene ring (lignin/carboxyl-rich acyclic molecules) (Liu et al., 2014), because formulas with DBE > 4 may contain one or more benzene rings. Moreover, DBE_{wa} decreased from 2.35 to 0.63 after light irradiation, indicating that the generated P-containing formulas became more saturated and nonaromatic (e.g., protein- and carbohydrate-like P-containing formula compounds); this also explains the sharp decrease in AI_{wa} and DBE_{wa} (Table S5). This result also corresponded to that of the P-containing formulas presented in Fig. 5. P-containing formulas had a CN range of 6–27 before light irradiation. After light irradiation, formulas with CNs > 15 were largely removed and the average CNs decreased, suggesting a decrease in the average molecular weight of P-containing formulas (Table S5) and indicating the breakage of C-O-P and/or C-P bonds by light irradiation.

The P-containing formulas removed after light irradiation were characterized by a low oxygen content (Fig. 5), while the generated P-containing formulas were rich in oxygen and highly saturated. The removed P-containing formulas mainly included lipid-like P-containing formula compounds with a low oxygen content and some saturation, unsaturated hydrocarbon-like P-containing formula compounds with low unsaturation, and lignin-like P-containing formula compounds with a low oxygen content (Fig. 4). As lipids are usually related to algae-derived OM with high

bioavailability (Liu et al., 2020), they can be easily removed after light irradiation. Previous studies considered lignin-like OM to be resistant (Hertkorn et al., 2006; Mesfioui et al., 2012; Opsahl and Benner, 1997; Yuan et al., 2017). However, we found that part of the lignin-like P-containing formula compounds were degraded after light irradiation (cf. blue spheres in zone 5; Fig. 5), implying that lignin-like P-containing formula compounds were not completely inert and their reactivity could be related to their molecular structure. In contrast, lignin-like P-containing formula compounds with high O/C (pink spheres in Fig. 5) were produced after light irradiation. These results suggest that lignin-like P-containing formula compounds with a low oxygen content are more photosensitive than those with a high oxygen content. The relationship between the light sensitivity of lignin-like P-containing formula compounds and their molecular structures should be further investigated in future studies. The generated P-containing formulas were mainly protein- and carbohydrate-like P-containing formula compounds, i.e., biolabile compounds and semibiolabile compounds freshly generated in surface waters (Chen et al., 2014; Wagner et al., 2015). In brief, P-containing formulas generated after light irradiation have a high oxygen content, high saturation, and low aromaticity.

3.3. Role of ROS

ROS play an important role in the element cycle of aquatic systems (Cory et al., 2010). Particularly, $^{3}CDOM^{*}$, •OH, H_2O_2, $^{1}O_2$, and $O_2^{\bullet-}$ are associated with the transformation of OM in water under light irradiation (Li et al., 2015; McNeill and Canonica, 2016; Mostafa and Rosario-Ortiz, 2013; Page et al., 2011; Wang et al., 2021;

Zhang et al., 2014). To assess the effects of ROS on POM photodegradation, a series of ROS capture experiments were performed. As shown in Fig. 7, the release of DIP decreased to varying degrees after adding various free-radical scavengers. After adding TMP (a $^3CDOM^*$ scavenger), the release of DIP decreased by 59.2%. After adding IPA (an •OH scavenger) and CAT (an H_2O_2 scavenger), the release of DIP decreased by 38.8% and 32.6%, respectively. The order of contribution of each ROS was as follows: $^3CDOM^* > •OH > H_2O_2 > {}^1O_2 > O_2^{•-}$. Fig. S9 presents the time evolution of H_2O_2, $O_2^{•-}$, PBA, FFA (a probe of $^1O_2$), and TMP (a probe of $^3CDOM^*$). During dark treatment, there was no obvious transformation of probe molecules, which was observed in ultrapure water (especially for FFA and TMP). The steady-state concentrations and formation rates of $^1O_2$ and $^3CDOM^*$ are summarized in Table S6. The steady-state concentrations and formation rates were 1.51×10^{-13} M and 0.76×10^{-7} M/s, respectively, for $^3CDOM^*$ and 0.43×10^{-12} M and 0.11×10^{-6} M/s, respectively, for $^1O_2$ in suspension, being much lower than those in filtered lake water. This indicates that the presence of particles hinders the production of $^1O_2$ and $^3CDOM^*$ or that the generated $^1O_2$ and $^3CDOM^*$ are rapidly absorbed by particles. However, opposite results were observed for •OH. The accumulated •OH content gradually increased with an increase in illumination time, and those in suspension were higher than those in filtered lake water. Thus, •OH plays an important role in the photorelease of DIP. Previous studies have revealed that both DOP and particulate organic phosphorus (POP) can be photolyzed to release DIP (Li et al., 2022; Zhang et al., 2019). The release of DIP from DOP is caused by the cleavage of P-O bonds by •OH (Zhao et al., 2018).

During the photodegradation of POM, we found that the release of DIP was accompanied by an increase in DOP concentration (Fig. S4). Hence, it can be inferred that POP in POM is first converted to DOP and DOP is then oxidized to produce DIP.

In general, •OH is the main ROS affecting the photochemical transformation of OM in water (Goldstone et al., 2002). We previously found that the photolytic release of P in water significantly decreased after adding an •OH scavenger (Li et al., 2017b). However, this phenomenon is different in lakes with different trophic states. In mesotrophic lakes, NO_3^- is the main contributor of •OH in water. With the proliferation of lake eutrophication, dissolved organic matter (DOM) gradually becomes the main contributor of •OH in water bodies (Guo et al., 2020). Lake Nanhu, selected in this experiment, is severely affected by eutrophication, and DOM is the main contributor to •OH generation in this lake. Notably, the photochemical reaction of DOM does not directly generate •OH. Instead, it first generates $^3CDOM^*$ under light irradiation and then generates •OH, H_2O_2, $^1O_2$, and $O_2^{\bullet-}$ through a series of reactions (Sharpless and Blough, 2014). The addition of TMP cuts off the subsequent reaction process, thereby inhibiting the photolytic release of dissolved phosphate.

3.4 Environmental implications

POM generally exists in various natural aquatic ecosystems, and its source and composition are extremely complex. It can be divided into exogenous and endogenous types. Exogenous POM mainly includes terrestrial plant debris and OM discharged by human activities and carried by rivers; its flux into lakes exhibits great variability. Endogenous POM is mainly produced by the residues of phytoplankton, large aquatic

426 plants, animals, and their metabolites. In previous studies, POM and DOM were mainly
427 distinguished according to their particle size (Azam and Malfatti, 2007; Roulet and
428 Moore, 2006). However, this classification does not fully reflect the chemical
429 characteristics, biological characteristics, and ecological functions. In fact, part of the
430 POM in aquatic ecosystems is relatively stable and difficult to decompose. It hardly
431 participates in the ecological process. In contrast, the other part is very active and has
432 an abnormally rapid turnover rate. This rapid transformation and degradation have an
433 important impact on the distribution pattern of nutrients and the recycling process.
434 However, understanding of the structural composition, degradation rate, and
435 transformation mechanism of POM in aquatic ecosystems is limited, resulting in a lack
436 of important links and basis for objectively describing the eutrophication process and
437 in turn controlling water bloom.

438 In eutrophic shallow lakes, excessive phytoplankton growth results in a large
439 amount of suspended POM. With the growth of phytoplankton, dissolved inorganic
440 nutrients are gradually consumed, and the mineralization and decomposition of POM
441 become an important nutrient compensation source. We found that POM exposed to
442 light irradiation could be photodegraded and DIP could be subsequently released. FT-
443 ICR MS revealed that the average molecular weight of P-containing formulas in POM
444 significantly decreased after light irradiation. P species in POM with lower oxidation
445 degrees and/or unsaturation were preferentially photodegraded, resulting in the
446 generation of species with higher oxidation degrees and more saturation (such as
447 protein- and carbohydrate-like P-containing formula compounds). $^{3}CDOM^{*}$ was

chiefly responsible for the photodegradation of POM. With the intensification of lake eutrophication, the easily degradable components of POM and the yield of $^{3}CDOM^{*}$ photo induced by DOM increase. The interaction between POM and $^{3}CDOM^{*}$ can lead to the rapid degradation of P species and their transformation into DIP, thereby exacerbating the P transformation rate in a water body. This indicates the importance of focusing on the continuous supply of endogenous P to study eutrophication and control blooms occurring in shallow lakes.

4. Conclusions

This study investigated the mechanism underlying DIP release during POM photodegradation using EEM and FT-ICR MS. POM in suspension was photodegraded and released DIP under light irradiation, and OP in POM participated in the photochemical reactions. The photodegradable P-containing formulas were mainly characterized by a lower oxidation degree and unsaturation. Meanwhile, some new P-containing formula compounds, particularly protein- and carbohydrate-like P-containing formulas that had a high oxygen content and were saturated, were photogenerated. $^{3}CDOM^{*}$ was the main ROS that played an important role in the photodegradation of POM. These results provide new insights into the biogeochemical cycle of POM and P in aquatic ecosystems and may further deepen our understanding of algal blooms in shallow lakes.

Acknowledgments

This research was supported by the National Natural Science Foundation of China (41877461), Fundamental Research Funds for the Central Universities

(2662020ZHPY002, 2662021ZH004), and Natural Science Foundation of Guangxi Province of China (2020GXNSFAA297080). We also acknowledge Dr. Chen He from China University of Petroleum-Beijing for her help in FT-ICR MS detection and analysis. Thanks to eceshi (www.eceshi.com) for the flow cytometry test.

References

Azam, F., Malfatti, F., 2007. Microbial structuring of marine ecosystems. Nat. Rev. Microbiol. 5 (10), 782-791.

Bae, E., Yeo, I.J., Jeong, B., Shin, Y., Shin, K.H., Kim, S., 2011. Study of double bond equivalents and the numbers of carbon and oxygen atom distribution of dissolved organic matter with negative-mode FT-ICR MS. Anal. Chem. 83 (11), 4193-4199.

Bahureksa, W., Tfaily, M.M., Boiteau, R.M., Young, R.B., Logan, M.N., McKenna, A.M., Borch, T., 2021. Soil organic matter characterization by Fourier transform ion cyclotron resonance mass spectrometry (FTICR MS): A critical review of sample preparation, analysis, and data interpretation. Environ. Sci. Technol. 55, 9637-9656.

Baldwin, D.S., beattie, J.K., Coleman, L.M., Jones, D.R., 1995. Phosphate ester hydrolysis facilitated by mineral phases. Environ. Sci. Technol. 29 (6), 1706-1709.

Benitez-Nelson, C.R., 2000. The biogeochemical cycling of phosphorus in marine systems. Earth-Science Rev. 51, 109-135.

Brooker, M.R., Longnecker, K., Kujawinski, E.B., Evert, M.H., Mouser, P.J., 2018. Discrete organic phosphorus signatures are evident in pollutant sources within a Lake Erie Tributary. Environ. Sci. Technol. 52 (12), 6771-6779.

Chen, H., Stubbins, A., Perdue, E.M., Green, N.W., Helms, J.R., Mopper, K., Hatcher, P.G., 2014. Ultrahigh resolution mass spectrometric differentiation of dissolved organic matter isolated by coupled reverse osmosis-electrodialysis from various major oceanic water masses. Mar. Chem. 164, 48-59.

Chen, N., Huang, Y., Hou, X., Ai, Z., Zhang, L., 2017. Photochemistry of hydrochar: Reactive oxygen species generation and sulfadimidine degradation. Environ. Sci. Technol. 51, 11278-11287.

Conley, D.J., Peaerl, H.W., Howarth, R.W., Boesch, D.F., Seitzinger, S.P., Havens, K.E., Lancelott, C., Likens, G.E., 2009. Controlling eutrophication: Nitrogen and phosphorus. Science 323, 1014-1015.

Cory, R.M., McNeill, K., Cotner, J.P., Amado, A., Purcell, J.M., Marshall, A.G., 2010. Singlet oxygen in the coupled photochemical and biochemical oxidation of dissolved organic matter. Environ. Sci. Technol. 44 (10), 3683-3689.

Feng, L., Xu, J., Kang, S., Li, X., Li, Y., Jiang, B., Shi, Q., 2016. Chemical composition of microbe-derived dissolved organic matter in cryoconite in Tibetan Plateau glaciers: Insights from Fourier transform ion cyclotron resonance mass spectrometry analysis. Environ. Sci. Technol. 50 (24), 13215-13223.

Gao, S.X., Zhang, X., Fan, W.Y., Sheng, G.P., 2021. Molecular insight into the variation of dissolved organic phosphorus in a wastewater treatment plant. Water Res. 203, 117529.

Goldstone, J.V., Pullin, M.J., Bertilsson, S., Voelker, B.M., 2002. Reactions of hydroxyl radical with humic substances: Bleaching, mineralization, and production of bioavailable carbon substrates. Environ. Sci. Technol. 36 (3), 364-372.

Guo, M., Li, X., Song, C., Liu, G., Zhou, Y., 2020. Photo-induced phosphate release during sediment resuspension in shallow lakes: A potential positive feedback mechanism of eutrophication. Environ. Pollut. 258, 113679.

Harfmann, J.L., Avery, G.B., Rainey, H.D., Mead, R.N., Skrabal, S.A., Kieber, R.J., Felix, J.D., Helms, J.R., Podgorski, D.C., 2021. Composition and lability of photochemically released dissolved organic matter from resuspended estuarine sediments. Org. Geochem. 151, 104164.

He, W., Chen, M., Park, J.E., Hur, J., 2016. Molecular diversity of riverine alkaline-extractable sediment organic matter and its linkages with spectral indicators and molecular size distributions. Water Res. 100, 222-231.

Helms, J.R., Glinski, D.A., Mead, R.N., Southwell, M.W., Avery, G.B., Kieber, R.J., Skrabal, S.A., 2014. Photochemical dissolution of organic matter from resuspended sediments: Impact of source and diagenetic state on photorelease. Org. Geochem. 73, 83-89.

Hertkorn, N., Benner, R., Frommberger, M., Schmitt-Kopplin, P., Witt, M., Kaiser, K., Kettrup, A., Hedges, J.I., 2006. Characterization of a major refractory component of marine

528 dissolved organic matter. Geochim. Cosmochim. Acta 70 (12), 2990-3010.
529 Hou, X., Feng, L., Dai, Y., Hu, C., Gibson, L., Tang, J., Lee, Z., Wang, Y., Cai, X., Liu, J.,
530 Zheng, Y., Zheng, C., 2022. Global mapping reveals increase in lacustrine algal blooms
531 over the past decade. Nat. Geosci. 15 (2), 130-134.
532 Hu, B., Wang, P., Bao, T., Qian, J., Wang, X., 2021. Mechanisms of photochemical release of
533 dissolved organic matter and iron from resuspended sediments. J. Environ. Sci. 104,
534 288-295.
535 Hu, B., Wang, P., Wang, C., Bao, T., 2022. Photogeochemistry of particulate organic matter in
536 aquatic systems: A review. Sci. Total Environ. 806 (Pt 3), 150467.
537 Hughey, C.A., Hendrickson, C.L., Rodgers, R.P., Marshall, A.G., Qian, K., 2001. Kendrick
538 mass defect spectrum: A compact visual analysis for ultrahigh-resolution broadbangd
539 mass spectra. Anal. Chem. 73 (19), 4676-4681.
540 Joshi, S.R., Kukkadapu, R.K., Burdige, D.J., Bowden, M.E., Sparks, D.L., Jaisi, D.P., 2015.
541 Organic matter remineralization predominates phosphorus cycling in the mid-Bay
542 sediments in the Chesapeake Bay. Environ. Sci. Technol. 49 (10), 5887-5896.
543 Kellerman, A.M., Kothawala, D.N., Dittmar, T., Tranvik, L.J., 2015. Persistence of dissolved
544 organic matter in lakes related to its molecular characteristics. Nat. Geosci. 8, 454-457.
545 Kim, S., Kramer, R.W., Hatcher, P.G., 2003. Graphical method for analysis of ultrahigh-
546 resolution broadband mass spectra of natural organic matter, the van Krevelen diagram.
547 Anal. Chem. 75, 5336-5344.
548 Klein, A.R., Bone, S.E., Bakker, E., Chang, Z., Aristilde, L., 2019. Abiotic phosphorus
549 recycling from adsorbed ribonucleotides on a ferrihydrite-type mineral: Probing
550 solution and surface species. J. Colloid Interf. Sci. 547, 171-182.
551 Lee, H.S., Hur, J., Shin, H.S., 2021. Dynamic exchange between particulate and dissolved
552 matter following sequential resuspension of particles from an urban watershed under
553 photo-irradiation. Environ. Pollut. 283, 117395.
554 Lee, H.S., Hur, J., Shin, H.S., 2023. Photochemical and microbial transformation of particulate
555 organic matter depending on its source and size. Sci. Total Environ. 857 (Pt 2), 159506.
556 Li, J.Y., Reardon, P., McKinley, J.P., Joshi, S.R., Bai, Y.G., Bear, K., Jaisi, D.P., 2017a. Water
557 column particulate matter: A key contributor to phosphorus regeneration in a coastal

eutrophic environment, the Chesapeake Bay. J. Geophys. Res.: Biogeosci. 122, 737-752.

Li, X., Guo, M., Duan, X., Zhao, J., Hua, Y., Zhou, Y., Liu, G., Dionysiou, D.D., 2019. Distribution of organic phosphorus species in sediment profiles of shallow lakes and its effect on photo-release of phosphate during sediment resuspension. Environ. Int. 130, 104916.

Li, X., Guo, M., Wang, Y., Liu, G., Fu, Q., 2022. Molecular insight into the release of phosphate from dissolved organic phosphorus photo-mineralization in shallow lakes based on FT-ICR MS analysis. Water Res. 222, 118859.

Li, X.L., Zhou, Y.Y., Liu, G.L., Lei, H.J., Zhu, D.W., 2017b. Mechanisms of the photochemical release of phosphate from resuspended sediments under solar irradiation. Sci. Total Environ. 595, 779-786.

Li, Y., Niu, J., Shang, E., Crittenden, J.C., 2015. Synergistic photogeneration of reactive oxygen species by dissolved organic matter and C_{60} in aqueous phase. Environ. Sci. Technol. 49 (2), 965-973.

Liu, F.J., Wei, X.Y., Xie, R.L., Wang, Y.G., Li, W.T., Li, Z.K., Li, P., Zong, Z.M., 2014. Characterization of oxygen-containing species in methanolysis products of the extraction residue from Xianfeng lignite with negative-ion electrospray ionization fourier transform ion cyclotron resonance mass spectrometry. Energ. Fuel. 28 (9), 5596-5605.

Liu, Q., Shank, G.C., 2015. Solar radiation-enhanced dissolution (photodissolution) of particulate organic matter in Texas estuaries. Estuar. Coast. 38 (6), 2172-2184.

Liu, S., He, Z., Tang, Z., Liu, L., Hou, J., Li, T., Zhang, Y., Shi, Q., Giesy, J.P., Wu, F., 2020. Linking the molecular composition of autochthonous dissolved organic matter to source identification for freshwater lake ecosystems by combination of optical spectroscopy and FT-ICR-MS analysis. Sci. Total Environ. 703, 134764.

Mayer, L.M., Schick, L.L., Skorko, K., 2006. Photodissolution of particulate organic matter from sediments. Limnol. Oceanogr. 51 (2), 1064-1071.

McDonough, L.K., Andersen, M.S., Behnke, M.I., Rutlidge, H., Oudone, P., Meredith, K., O'Carroll, D.M., Santos, I.R., Marjo, C.E., Spencer, R.G.M., McKenna, A.M., Baker,

588 A., 2022. A new conceptual framework for the transformation of groundwater
589 dissolved organic matter. Nat. Commun. 13 (1), 2153.
590 McNeill, K., Canonica, S., 2016. Triplet state dissolved organic matter in aquatic
591 photochemistry: Reaction mechanisms, substrate scope, and photophysical properties.
592 Environ. Sci.: Processes Impacts 18 (11), 1381-1399.
593 Mesfioui, R., Love, N.G., Bronk, D.A., Mulholland, M.R., Hatcher, P.G., 2012. Reactivity and
594 chemical characterization of effluent organic nitrogen from wastewater treatment
595 plants determined by Fourier transform ion cyclotron resonance mass spectrometry.
596 Water Res. 46 (3), 622-634.
597 Mostafa, S., Rosario-Ortiz, F.L., 2013. Singlet oxygen formation from wastewater organic
598 matter. Environ. Sci. Technol. 47 (15), 8179-8186.
599 Murphy, J., Riley, J.P., 1962. A modified single solution method for the determination of
600 phosphate in natural waters. Anal. Chim. Acta 27, 31-36.
601 Ni, Z., Li, Y., Wang, S., 2022. Cognizing and characterizing the organic phosphorus in lake
602 sediments: Advances and challenges. Water Res. 220, 118663.
603 Ni, Z., Xiao, M., Luo, J., Zhang, H., Zheng, L., Wang, G., Wang, S., 2021. Molecular insights
604 into water-extractable organic phosphorus from lake sediment and its environmental
605 implications. Chem. Eng. J. 416, 129004.
606 Ohno, T., HE, Z., Sleighter, R.L., Honeycutt, C.W., Hatcher, P.G., 2010. Ultrahigh resolution
607 mass spectrometry and indicator species analysis to identify marker components of
608 soil- and plant biomass- derived organic matter fractions. Environ. Sci. Technol. 44
609 (22), 8594-8600.
610 Opsahl, S., Benner, R., 1997. Distribution and cycling of terrigenous dissolved organic matter
611 in the ocean. Nature 386, 480-482.
612 Page, S.E., Arnold, W.A., McNeill, K., 2011. Assessing the contribution of free hydroxyl radical
613 in organic matter-sensitized photohydroxylation reactions. Environ. Sci. Technol. 45
614 (7), 2818-2825.
615 Riedel, T., Biester, H., Dittmar, T., 2012. Molecular fractionation of dissolved organic matter
616 with metal salts. Environ. Sci. Technol. 46 (8), 4419-4426.
617 Roulet, N., Moore, T.R., 2006. Environmental chemistry: Browning the waters. Nature 444,

283-284.

Rydin, E., 2000. Potentially mobile phosphorus in Lake Erken sediment. Water Res. 34 (7), 2037-2042.

Schindler, D.W., Carpenter, S.R., Chapra, S.C., Hecky, R.E., Orihel, D.M., 2016. Reducing phosphorus to curb lake eutrophication is a success. Environ. Sci. Technol. 50 (17), 8923-8929.

Shank, G.C., 2011. Solar radiation enhanced dissolution of particulate organic matter from coastal. Limnol. Oceanogr. 56 (2), 577-588.

Sharpless, C.M., Blough, N.V., 2014. The importance of charge-transfer interactions in determining chromophoric dissolved organic matter (CDOM) optical and photochemical properties. Environ. Sci.: Processes Impacts 16, 654-671.

Singer, G.A., Fasching, C., Wilhelm, L., Niggemann, J., Steier, P., Dittmar, T., Battin, T.J., 2012. Biogeochemically diverse organic matter in Alpine glaciers and its downstream fate. Nat. Geosci. 5, 710-714.

Song, N., Jiang, H.L., 2020. Coordinated photodegradation and biodegradation of organic matter from macrophyte litter in shallow lake water: Dual role of solar irradiation. Water Res. 172, 115516.

Wagner, S., Riedel, T., Niggemann, J., Vahatalo, A.V., Dittmar, T., Jaffe, R., 2015. Linking the molecular signature of heteroatomic dissolved organic matter to watershed characteristics in world rivers. Environ. Sci. Technol. 49, 13798-13806.

Wan, B., Huang, R., Diaz, J.M., Tang, Y., 2019. Polyphosphate adsorption and hydrolysis on aluminum oxides. Environ. Sci. Technol. 53, 9542-9552.

Wang, Z., Lv, J., Zhang, S., Christie, P., Zhang, S., 2021. Interfacial molecular fractionation on ferrihydrite reduces the photochemical reactivity of dissolved organic matter. Environ. Sci. Technol. 55 (3), 1769-1778.

Worsfold, P.J., Monbet, P., Tappin, A.D., Fitzsimons, M.F., Stiles, D.A., McKelvie, I.D., 2008. Characterisation and quantification of organic phosphorus and organic nitrogen components in aquatic systems: A review. Anal. Chim. Acta 624 (1), 37-58.

Xu, G., Sun, Z., Fang, W., Liu, J., Xu, X., Lv, C., 2018. Release of phosphorus from sediments under wave-induced liquefaction. Water Res. 144, 503-511.

Yuan, Z., He, C., Shi, Q., Xu, C., Li, Z., Wang, C., Zhao, H., Ni, J., 2017. Molecular insights into the transformation of dissolved organic matter in landfill leachate concentrate during biodegradation and coagulation processes using ESI FT-ICR MS. Environ. Sci. Technol. 51 (14), 8110-8118.

Zeng, Y., Fang, G., Fu, Q., Peng, F., Wang, X., Dionysiou, D.D., Guo, J., Gao, J., Zhou, D., Wang, Y., 2022. Mechanistic study of the effects of agricultural amendments on photochemical processes in paddy water during rice growth. Environ. Sci. Technol. 56 (7), 4221-4230.

Zhang, D., Yan, S., Song, W., 2014. Photochemically induced formation of reactive oxygen species (ROS) from effluent organic matter. Environ. Sci. Technol. 48 (21), 12645-12653.

Zhang, L., Chen, M., Zheng, Y., Wang, J., Xiao, X., Chen, X., Hu, C., Shen, J., Liu, J., Tang, K., Xu, D., Shi, Q., Ning, X., Thomas, H., Qin, W., Zhao, M., Jiao, N., Zhang, Y., 2022a. Microbially driven fate of terrigenous particulate organic matter in oceans. Limnol. Oceanogr. 9999, 1-17.

Zhang, X., Li, J., Fan, W.Y., Sheng, G.P., 2019. Photomineralization of effluent organic phosphorus to orthophosphate under simulated light illumination. Environ. Sci. Technol. 53, 4997-5004.

Zhang, Y., Deng, J., Qin, B., Zhu, G., Zhang, Y., Jeppesen, E., Tong, Y., 2022b. Importance and vulnerability of lakes and reservoirs supporting drinking water in China. Fundamental Research 10.1016/j.fmre.2022.01.035.

Zhao, J.W., Jiang, Y.C., Kong, M.H., Liu, G.L., Dionysiou, D.D., 2018. Fe(III)-oxalate complex mediated phosphate released from diazinon photodegradation: Pathway signatures based on oxygen isotopes. J. Hazard. Mater. 358, 319-326.

Zheng, N., He, X., Hu, R., Wang, R., Zhou, Q., Lian, Y., Hu, Z., 2022. In-situ production of singlet oxygen by dioxygen activation on iron phosphide for advanced oxidation processes. Appl. Catal. B-Environ. 307, 121157.

Zhu, Y.R., Wu, F.C., He, Z.Q., Guo, J.Y., Qu, X.X., Xie, F.Z., Giesy, J.P., Liao, H.Q., Guo, F., 2013. Characterization of organic phosphorus in lake sediments by sequential fractionation and enzymatic hydrolysis. Environ. Sci. Technol. 47 (14), 7679-7687.

678 Zong, Y., Mao, Y., Xu, L., Wu, D., 2020. Non-selective degradation of organic pollutants via
679 dioxygen activation induced by Fe(II)-tetrapolyphosphate complexes: Identification of
680 reactive oxidant and kinetic modeling. Chem. Eng. J. 398, 125603.
681

Figure

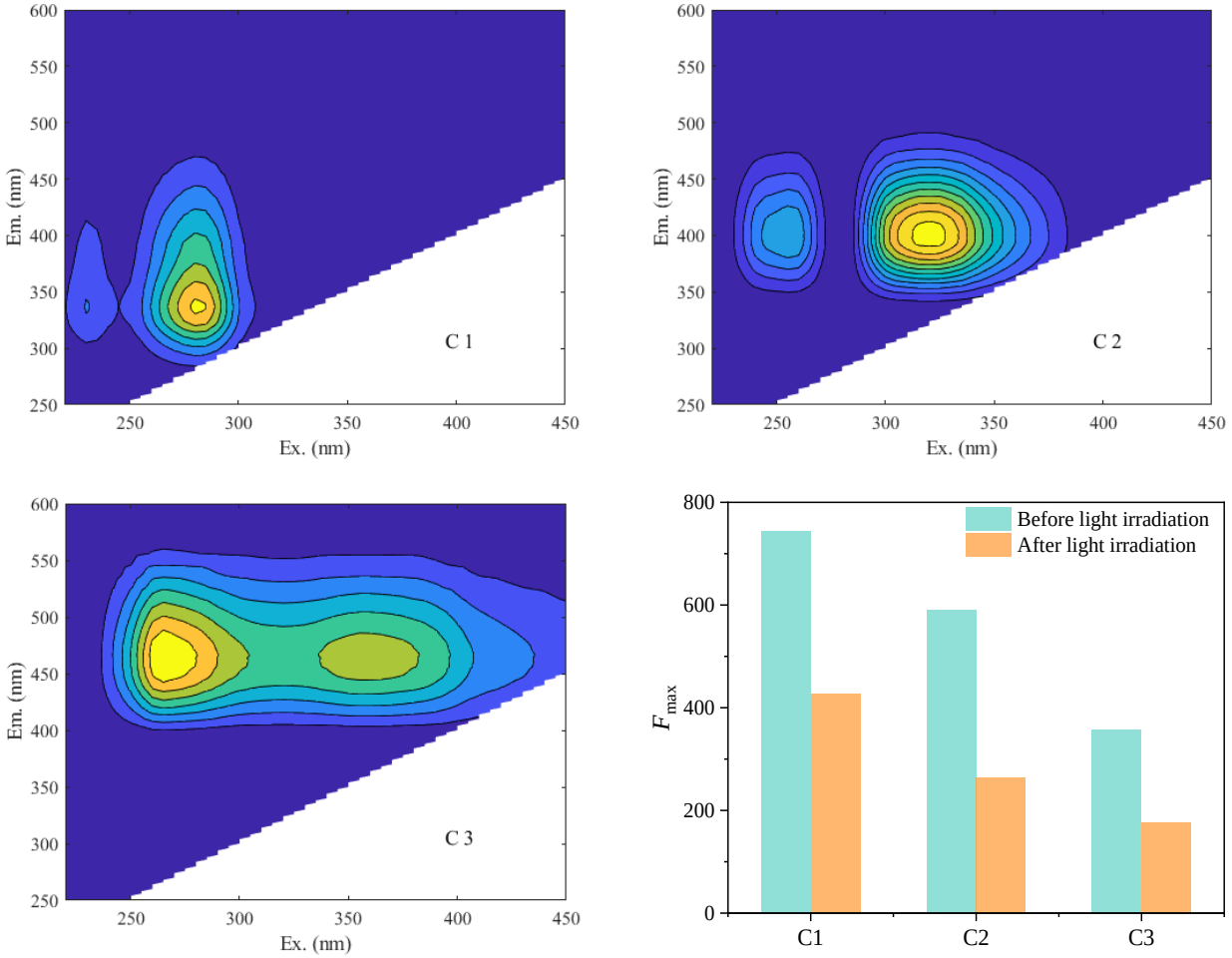

Fig. 1. The three fluorescent components of POM identified by EEM-PARAFAC modeling (C1-C3, respectively) and their F_{max} before and after light irradiation.

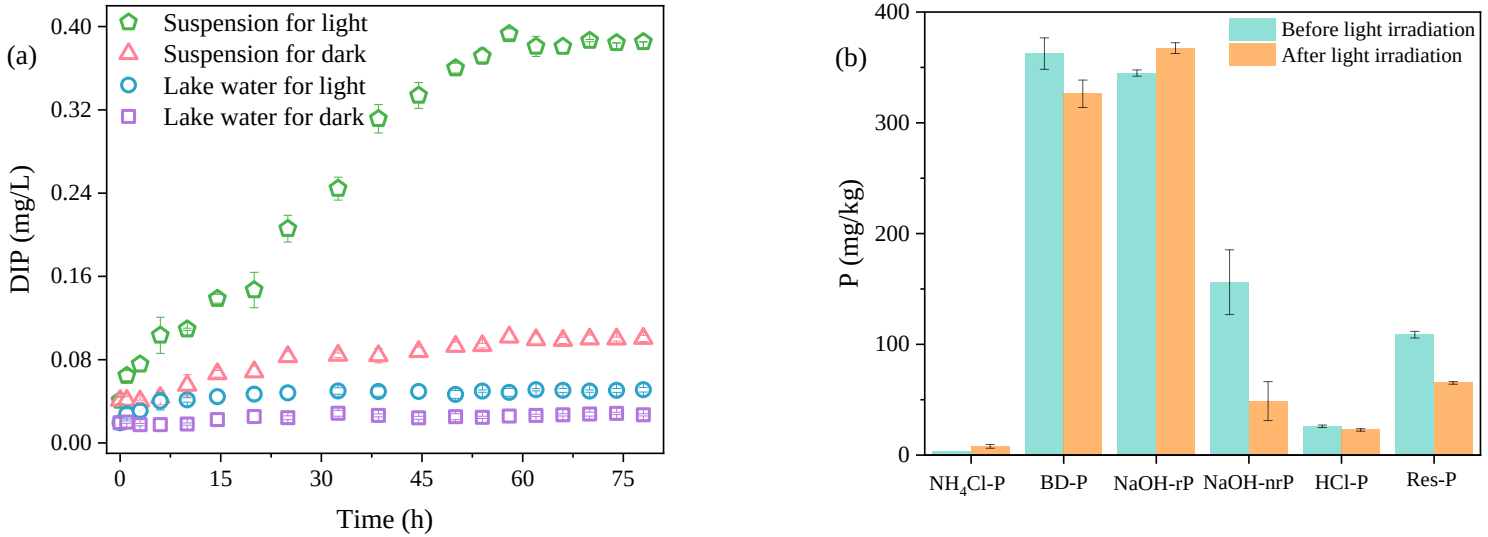

Fig. 2. (a) The concentration changes of DIP in filtered lake water and suspension under light irradiation or dark treatment; (b) Changes of P fractions in POM obtained from suspension solution before and after light irradiation.

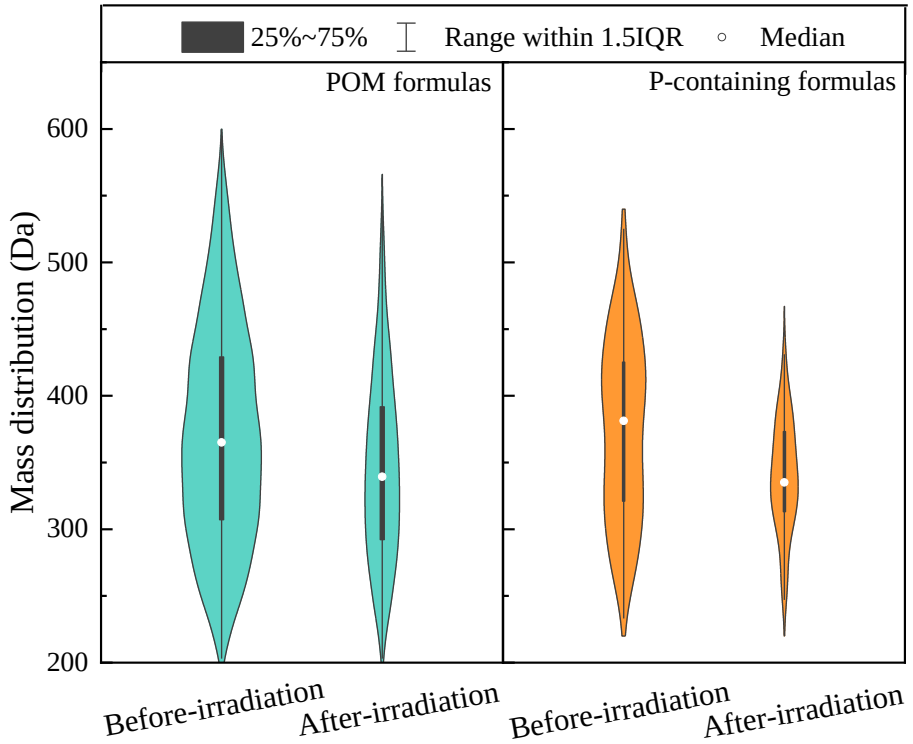

Fig. 3. Mass distributions of POM and P-containing formulas before and after light irradiation

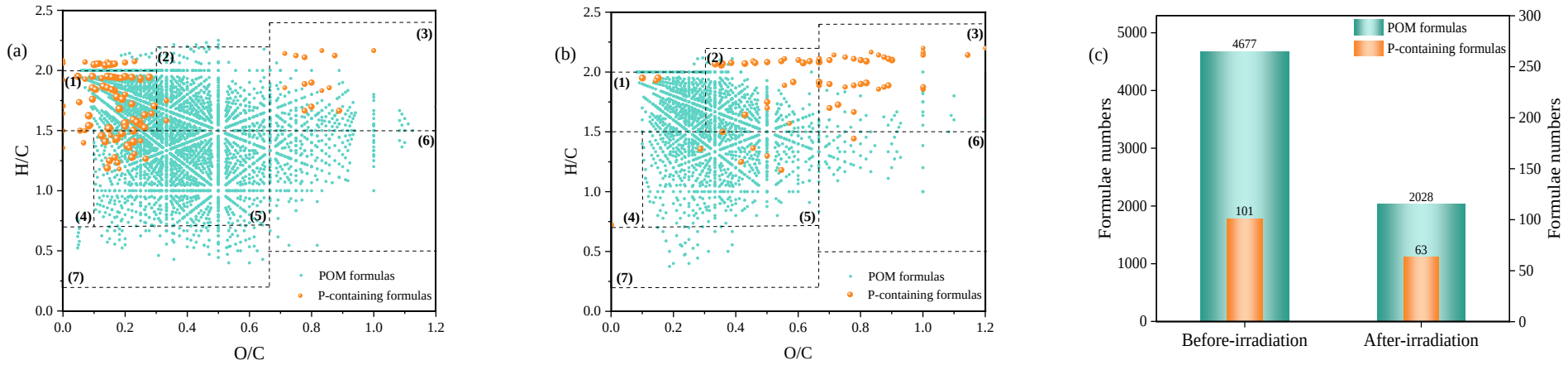

Fig. 4. Van Krevelen diagrams from the mass spectra of POM and P-containing formulas before (a) and after (b) light irradiation and their formulae numbers distribution change (c). The different boxes represent specific compound categories, including: (1) lipids-; (2) proteins-; (3) carbohydrates-; (4) unsaturated hydrocarbons-; (5) lignins-; (6) tannins-, and (7) condensed aromatic structures-like formula compounds. Blue dots represent POM formulas, and orange spheres represent P-containing formulas. The size of the orange spheres represents the molecular weight of P-containing formulas.

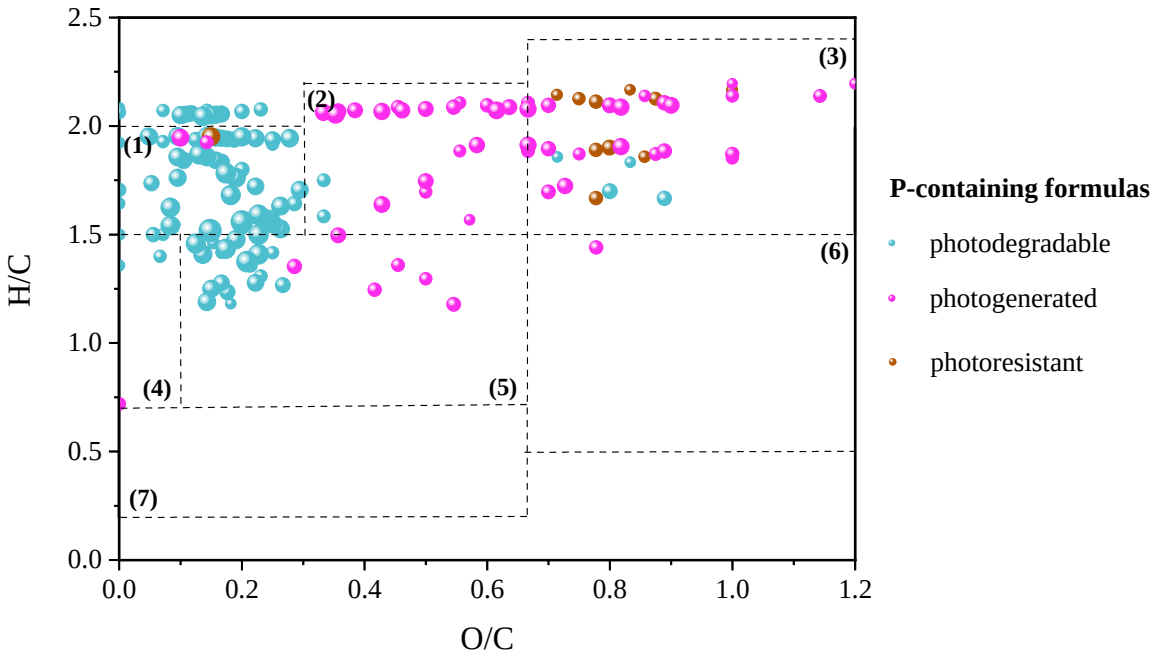

Fig. 5. Van Krevelen diagrams of photodegradable, photogenerated, and photoresistant P-containing formulas during POM photodegradation. The size of the sphere represents the molecular weight of each P-containing formula.

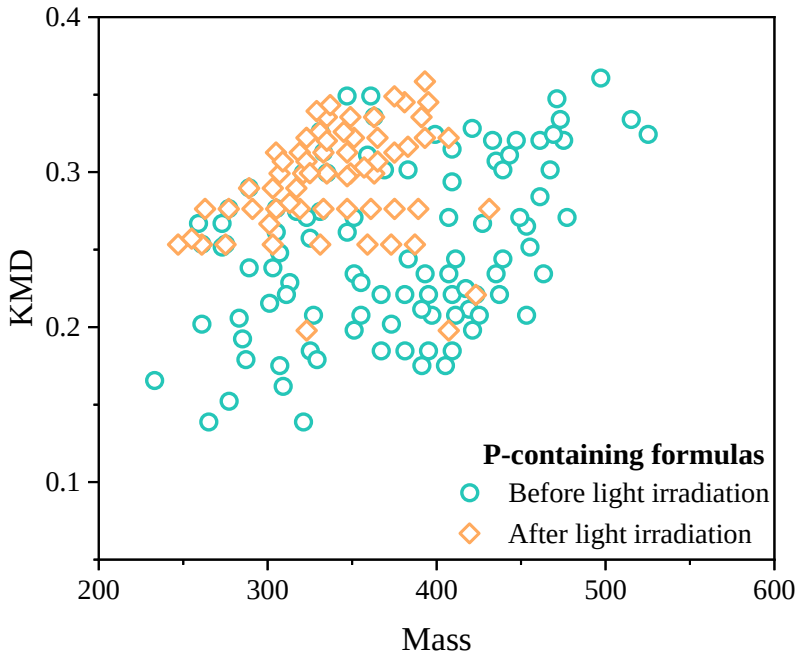

Fig. 6. Kendrick mass defect (KMD) analysis of P-containing formulas before (a) and after (b) light irradiation.

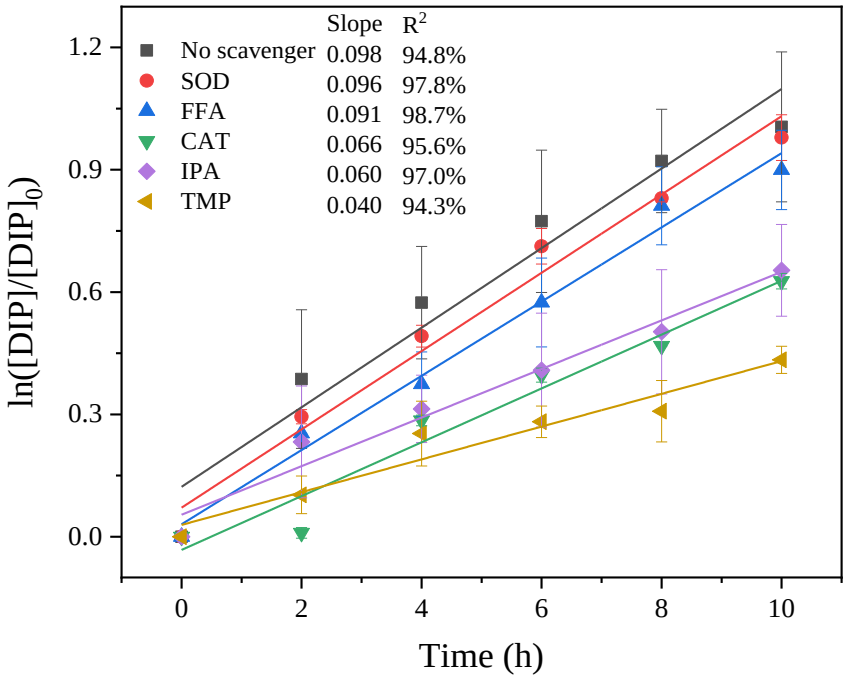

Fig. 7. The inhibition effect of different radical scavengers on the release of DIP during POM photodegradation (SOD for $O_2^{\bullet-}$, FFA for $^1O_2$, CAT for H_2O_2, IPA for •OH, TMP for $^3CDOM^*$).